JOURNAL OF GEOPHYSICAL RESEARCH, VOL. 100, NO. C4, PAGES 6605–6619, APRIL 15, 1995

Vertical structure of the upper ocean during the Marine Light–Mixed Layers experiment

Albert J. Plueddemann and Robert A. Weller
Woods Hole Oceanographic Institution, Woods Hole, Massachusetts

Malgorzata Stramska and Tommy D. Dickey
Ocean Physics Group, Department of Earth Sciences, University of Southern California, Los Angeles

John Marra
Lamont-Doherty Earth Observatory of Columbia University, Palisades, New York

Abstract. The Marine Light–Mixed Layers (MLML) experiments took place in the subarctic North Atlantic Ocean, approximately 275 miles south of Reykjavik, Iceland, during 1989 and 1991. The 1991 field program took place from April 30 to September 6 and included a central surface mooring to document the temporal evolution of physical, biological, and optical properties. In this paper we describe the physical variability observed at the 1991 mooring site, concentrating on the vertical structure of temperature and velocity in the upper 300 m of the water column and their changes in response to heat and momentum fluxes at the sea surface. The deployment period included the spring transition, when upper ocean restratification was initiated after deep winter mixing, and the fall transition, when mixed layer deepening began again. The dominant signal in temperature was seasonal variation, with a 6°C increase observed at the sea surface from May to August. Prior to development of the seasonal stratification, a period dominated by near-surface temperature variability was observed in association with a 15-day mean flux of only 20 W m^{-2} into the ocean. Pronounced day/night oscillations of heat flux during this period resulted in alternating development and destruction of stratification and intense diurnal cycling of the mixed layer depth. A qualitative comparison of the observed temperature structure to the prediction of a one-dimensional mixed layer model showed that local processes dominated during the initiation of restratification and during most of the summer warming period. Nonlocal processes were important after the fall transition.

1. Introduction

The subarctic North Atlantic is a region with strong seasonal signals in both physical and bio-optical properties [*Marra*, 1989]. The site chosen for the Marine Light–Mixed Layers (MLML) field program (Figure 1) is characterized by a deep (600–800 m) winter mixed layer [*Robinson et al.*, 1979; *Lambert and Hebenstreit*, 1985] as a result of substantial surface heat loss and strong wind forcing from September to March [*Isemer and Hasse*, 1985, 1987]. Of particular interest at this site is the spring restratification process, wherein the deep mixed layer shoals dramatically as a result of increased surface heating during periods of weak wind forcing. The seasonal changes in mixed layer depth result in immense changes in plankton biomass observed as the spring bloom [e.g., *Ducklow*, 1989].

It has been recognized for some time [e.g., *Sverdrup*, 1953] that the timing and extent of the spring bloom must be principally controlled by the restratification of the water column. However, as pointed out by *Ducklow* [1989], there are very few combined physical/bio-optical data sets that allow a detailed investigation of the process. A handful of such data sets have now been analyzed and are beginning to yield new insight regarding the extent to which bio-optical properties can be predicted, given knowledge of the surface forcing. In the simplest case the one-dimensional (vertical) upper ocean response to local surface forcing is separable from nonlocal effects like horizontal advection and mesoscale variability. In the general case, nonlocal effects may be significant [*Dickey et al.*, 1991, 1993; *Robinson et al.*, 1993], limiting the usefulness of one-dimensional, surface-forced modeling and leading to more complex analysis techniques [*McGillicuddy et al.*, 1995a, b]. However, due to the dominance of the seasonal cycle over mesoscale processes in the subarctic North Atlantic [*Gill*, 1975], the variability of the upper ocean during restratification can be predicted to first order by a one-dimensional model. The applicability of simple upper ocean models makes the MLML site particularly appealing for investigation of biological/physical coupling [*Stramska and Dickey*, 1993, 1994].

In this paper we present the air-sea fluxes of heat and momentum, and the vertical structure of temperature and currents in the upper 300 m of the water column observed at the MLML site during the spring and summer of 1991. Our intent is to provide the physical context in which the extensive bio-optical measurements from the MLML experiment were taken. The observations come from a heavily

Paper number 94JC03203.
0148-0227/95/94JC-03203$05.00

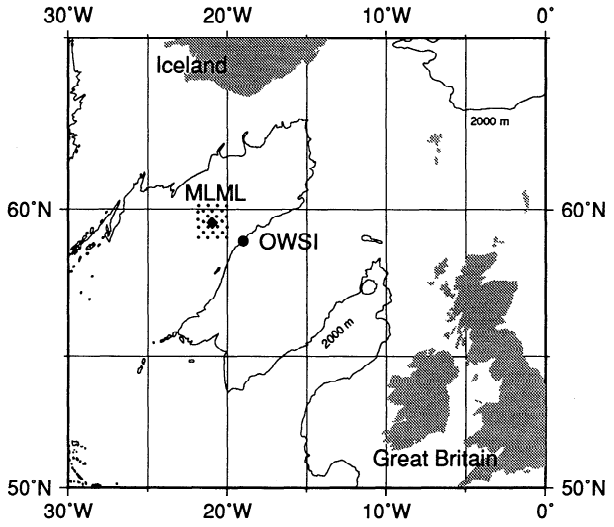

Figure 1. The MLML mooring site is shown along with a grid representing the shipboard survey region. The mooring was deployed at 59°35.61'N, 20°57.85'W in 2822 m of water about 275 mi south of Reykjavik, Iceland. The site at 59°N, 19°W is Ocean Weather Station India (OWSI), where the data of *Lambert and Hebenstreit* [1985] were collected.

instrumented surface mooring that served as the focal point for the 1991 MLML field program. The seasonal variability in temperature is discussed and compared with historical data from the region. The onset of restratification is considered in detail, focusing on a 15-day period of near-zero mean heat flux and strong oscillations of mixed layer depth which preceded the spring transition. The local response of the upper ocean to wind and thermal forcing is assessed qualitatively by comparing the observations to a one-dimensional mixed layer model.

2. Methods

2.1. The MLML Mooring

The MLML experimental site (Figure 1) was in a region characterized by high winds, large waves, and strong currents. This severe environment represented a challenge to our ability to make detailed measurements of local atmospheric forcing and the biological, optical, and physical variability of the upper ocean. The process of meeting this challenge began in 1989 with the design and deployment of the MLML pilot mooring. The pilot mooring was deployed in April of 1989 in anticipation of a 5-month deployment, but remained on station for only 10 weeks, after which the failure of a component in the mooring line caused the surface buoy to go adrift and the mooring line to sink to the bottom (both buoy and mooring line were later recovered). Despite these technical problems, the pilot mooring provided a unique high-latitude data set during restratification of the upper ocean and initiation of the spring bloom [*Dickey et al.*, 1994a; *Stramska and Dickey*, 1992, 1993, 1994].

Benefiting from extensive evaluation of the performance of the pilot mooring, the 1991 MLML mooring (Figure 2) was designed both to minimize the static tension along the mooring line and to survive peak tensions in excess of those observed in 1989 [*Plueddemann et al.*, 1993]. The new mooring design resulted in a reliable severe-environment platform from which 129 days of surface and subsurface data were collected between April 30 and September 6, 1991. The critical design elements of the 1991 mooring included upgraded hardware to survive cyclic loading, an increase in scope (the ratio of the slack length of the mooring to the water depth) to minimize static tension, and a compliant element that allowed the mooring to be "tuned," so that the resonant frequency was outside of the surface wave band. The 1991 mooring was of compound (wire, nylon, and polypropylene) construction, using a 10-ft-diameter discus buoy as a surface float. The scope of the mooring was 1.25. The mooring used the so-called "inverse catenary" design, wherein a section of negatively buoyant nylon was spliced to a section of positively buoyant polypropylene just above the

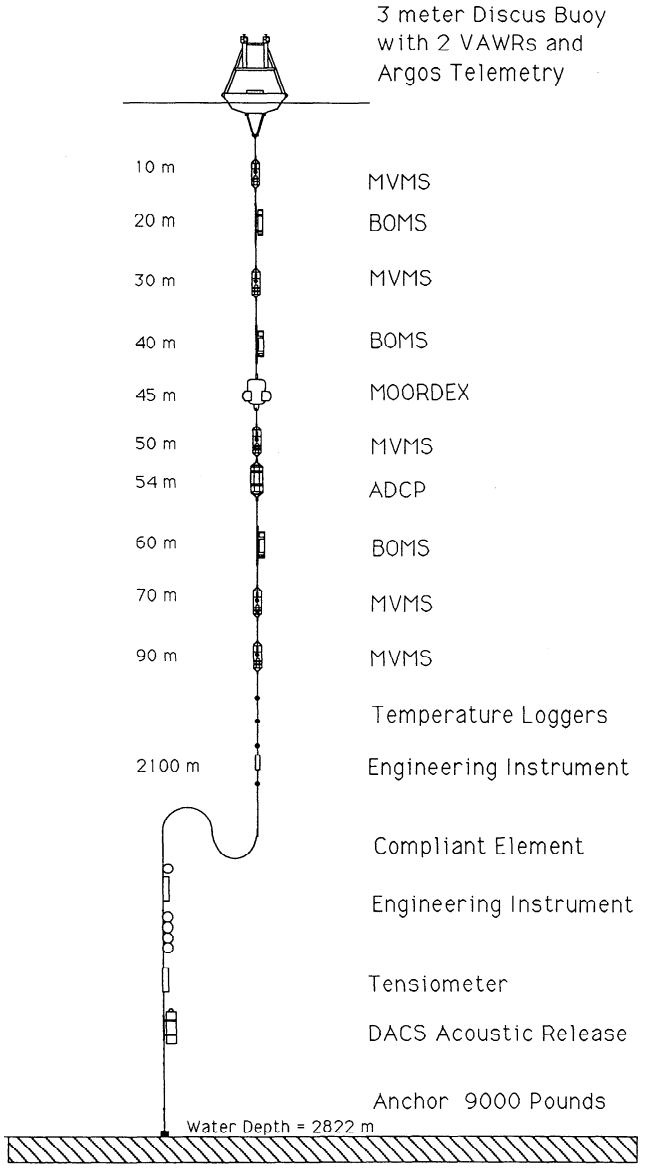

Figure 2. Schematic diagram of the 1991 MLML surface mooring. Instrumentation in the upper 90 m is described in the text. Temperature loggers were positioned at 80 m and at 16-m increments from 102- to 310-m depth. The engineering instruments measured tension, inclination, temperature, and depth. The compliant element consisted of 630 m of 7/8-inch nylon spliced to 670 m of $1\frac{1}{8}$-inch polypropylene.

flotation balls. At low current speeds, the nylon/polypro section took on an "S" shape (Figure 2). This allowed scopes significantly greater than 1, while eliminating the possible tangling problem of slack line in low currents.

The mooring was deployed and recovered by the R/V *Endeavor*, sailing out of Reykjavik, Iceland. *Endeavor* departed for the experimental site, approximately 275 mi south of Reykjavik, on April 27, 1991, and the mooring deployment was completed at 1600 UT on April 29. The anchor position was determined to be 59°35.61'N, 20°57.85'W in 2822 m of water. The recovery cruise was initiated on September 5, 1991, during a rare period of calm seas and low winds. Recovery was completed by 1800 UT on September 6.

2.2. Instrumentation

Instrumentation on the surface buoy included two vector averaging wind recorders (VAWR's) [*Dean and Beardsley*, 1988], an engineering instrument for sampling tension and vertical acceleration, and an Argos satellite communications system that transmitted VAWR data and buoy position. In addition to the Argos telemetry, the VAWR's recorded data internally at 15-min intervals. Both VAWR's were outfitted with sensors for the measurement of wind speed (WS), wind direction (WD), sea surface temperature (SST), air temperature (AT), incident shortwave (250–2500 nm) (SW) radiation, barometric pressure (BP), relative humidity (RH), and incident longwave (4–50 μm) (LW) radiation. The LW measurements from MLML are discussed by *Dickey et al.* [1994b] and will not be presented here. All of the VAWR sensors, except SST, were attached to the discus buoy tower at about 3-m height. The two SST sensors were attached to the buoy bridle at depths of approximately 1 m and 2 m.

Observations from the two VAWR's were compared by *Plueddemann et al.* [1993]. Sensor performance was evaluated by considering the statistics of the differences between like variables observed by the two VAWR's in comparison to the expected accuracy and precision of the sensors documented by *Weller et al.* [1990]. If the observed performance was poor, preexperiment and postexperiment calibration data were used to determine which sensor was causing the problem. The best performing sensor for each variable was chosen to form the "final" meteorological data set for computation of air-sea fluxes. In most cases, either the sensor pair performed within specifications (making the choice arbitrary) or the better performing sensor of the pair was easily identified.

There were three problems that could not be resolved with this approach: a large mean of the WD difference (4.6°), a large standard deviation of the AT difference (0.08°C), and a large mean (0.04°C) and standard deviation (0.47°C) of the SST difference between May 22 and July 31. The WD error was attributed to a compass calibration bias. The instrument with the better compass postcalibration was used. There were no indications of instrumental problems with the AT sensors, and the observed differences were attributed to small-scale variability in the true AT field. The mean value of AT from the two sensors was used in the final data set. Evaluation of the SST observations indicated a sensor malfunction, but the problem was transient in the data and was not evident in the postdeployment calibrations or electronics checks. It was not possible to determine the cause of the problem or to isolate it to a single sensor. For the final data set the SST sensor that appeared, subjectively, to have performed the best was used. Two ad hoc adjustments to the SST were made to minimize the difference between SST and the 10-m temperature record. Additive constants of +0.93°C and −0.64°C were applied near 0600 UTC on May 31 and 1000 UTC on June 14, respectively.

The upper 90 m of the mooring (Figure 2) was instrumented with a variety of multidisciplinary measurement systems, including five multivariable moored systems (MVMS's) [*Dickey*, 1991], three bio-optical moored systems (BOMS) [*Smith et al.*, 1991], and a moored bioluminescence sensor (MOORDEX). The bio-optical data from the MVMS's are discussed by *Stramska et al.* [this issue], and the MOORDEX results by *Neilson et al.* [this issue]. In this report, we used only the temperature and current measurements from the MVMS's deployed at 10-, 30-, 50-, and 70-m depth. The 90-m instrument recorded good current data only for the first three days of the deployment due to a compass failure and had a timing problem, which made the temperature data unreliable. The remaining data, recorded at either 1-min intervals (10- and 50-m depths) or 128-s intervals (30 and 70 m) were averaged to 15 min. The temperature records from 10, 50, and 70 m were complete, and no further processing was required. The record at 30 m had a gap between July 27 and August 26, and the 70-m record stopped on June 30. The missing data were filled using linear interpolation between their nearest neighbors in the vertical. The current records from 10, 50, and 70 m were complete, but the 30-m record stopped on July 9 due to a broken rotor. The missing 30-m currents were filled by interpolation between the 10-m and 50-m records.

Fifteen submersible temperature loggers (STL's) and an acoustic doppler current profiler (ADCP) were deployed to supplement the MVMS measurements below 50 m and to extend the range of current and temperature observations to 310-m depth. One STL was placed at 80-m depth, and the remaining 14 sensors were placed at 16-m intervals between 102-m and 310-m depth to match the center points of the averaged ADCP depth cells (see explanation below). Complete records were obtained from 11 of the 15 STL's, a partial record was obtained from the twelfth instrument, and no data were recovered from the remaining three. The partial record showed calibration drift and was eventually abandoned. The four failures left gaps in the temperature record at 134-m depth and between 246-m and 294-m depth.

Ten of the 11 STL's used in the analysis had good postdeployment calibrations and were found to be extremely stable (the mean difference in observed temperature using the predeployment and postdeployment calibration constants was 0.005° or less). Some problems were encountered with calibration of the other temperature sensors. A predeployment conductivity-temperature-depth (CTD) cast showed that the upper water column was initially well mixed, and the mooring temperatures showed very little variation over the first 16 hours. Thus we chose to make calibration adjustments by comparing the mooring temperatures averaged over the first 8 hours of April 30 to the temperature profile from the CTD cast (Figure 3). The CTD temperature profile varied by less than 0.04°C from the surface to 220-m depth and by less than 0.1°C to 270-m depth. The STL's above 220 m agreed with the CTD temperature to within about 0.015°C. The SST and the MVMS temperatures were suspect due to the high degree of depth-to-depth variability and poor agreement with the

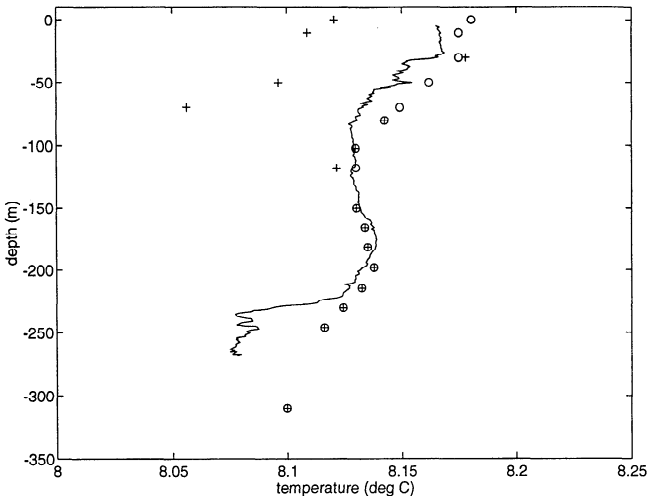

Figure 3. Mooring temperatures compared with the predeployment CTD cast. The CTD cast was taken at 0500 UT on April 29, just prior to the mooring deployment. The mooring temperatures were averaged over the first 8 hours of April 30. Crosses represent the raw mooring data, and circles represent the data after an ad hoc calibration adjustment. Depths where crosses and circles overlay represent instruments with good predeployment and postdeployment calibrations and no adjustment.

CTD. An ad hoc adjustment of the temperatures from sensors with suspect calibrations was made in order to bring the 8-hour means into reasonable agreement with the CTD and minimize inversions. The adjustment was applied as an additive constant to all temperatures in the record for a given instrument. After adjustment, temperatures from the mooring and the CTD cast agreed to within about 0.020° down to 220 m (Figure 3). Larger differences were seen below 220 m, but since the instruments in this depth range had good predeployment and postdeployment calibrations, they were not adjusted. We compared the adjusted mooring temperatures to CTD casts taken throughout the May sampling period and found that the adjustments substantially reduced the mean difference between the mooring and CTD temperatures.

The ADCP was a 150-kHz, self-contained unit outfitted with pendulum tilt sensors, a fluxgate compass, and 20 Mbytes of solid-state memory. The pressure case was clamped to a load cage with the transducers facing downward from a depth of 54 m. The ADCP was configured to send out transmissions at 1-s intervals for a period of 60 s. This sequence of 60 transmissions was repeated at 15-min intervals. The backscattered signal was processed over time intervals corresponding to an 8-m depth cell length, while the nominal depth resolution of the transmitted pulse was 16 m. Thus the data were oversampled in depth, and successive depth cells were not independent. Forty cells were recorded, but prior to analysis, the data were averaged in pairs, so that the sampling interval matched the 16-m depth resolution. Velocities were corrected for tilt and converted to geographic coordinates prior to ensemble averaging. The estimated lower-bound precision [*Theriault*, 1986] for the 15-min average horizontal velocities was about 0.6 cm s^{-1}. Experience has shown that actual performance is likely to be 2–3 times this lower bound. A comparison of the ADCP currents at 86 m and the MVMS currents at 50 and 70 m showed rms differences in speed of about 2 cm s^{-1} and in direction of about 7°. These differences were near the expected instrumental error level and comparable to differences between the 50-m and 70-m MVMS records. Coherence between the ADCP and MVMS's was significant out to a frequency of about 0.3 cph, where the ADCP spectra reached a noise floor.

2.3. Estimation of Air-Sea Fluxes

The air-sea fluxes of momentum and heat for the MLML experiment were computed from the meteorological variables using bulk aerodynamic formulae. Time series of wind stress, latent heat flux, and sensible heat flux were computed using the stability-dependent formulae of *Large and Pond* [1981, 1982]. Net shortwave radiation was computed from observed incoming shortwave by multiplying by $(1 - \alpha)$, with the albedo α taken as 0.06 [*Payne*, 1972]. Net longwave radiation was estimated by assuming nearly blackbody radiation [*Clarke et al.*, 1974] and correcting for the presence of clouds [*Fung et al.*, 1984]. The daytime cloud fraction was estimated by comparing theoretical clear-sky radiation to the observed shortwave radiation [*Plueddemann et al.*, 1993]. Nighttime values were interpolated between the nearest two daytime values, and the resulting cloud fraction record was smoothed over 30 hours to reduce sensitivity to the day/night transitions.

The results of the bulk flux computations were time series of wind stress, sensible and latent heat flux, net shortwave radiation, and cloud-corrected net longwave radiation. This formed a surface flux time series for MLML, which was complete except for precipitation. In an attempt to introduce realistic seasonal evaporation minus precipitation $(E - P)$ variability, a proxy for precipitation was developed from the historical data presented by *Schmitt et al.* [1989]. The MLML evaporation time series was first computed from the observed meteorological variables and averaged to monthly values. Monthly precipitation was then computed from the difference between monthly means of the observed evaporation and the monthly climatological $E - P$ values of Schmitt et al. Since the surface fluxes were desired on a uniform time grid for use with a time-stepped mixed layer model, the monthly precipitation time series was interpolated to 15-min intervals.

3. Results and Discussion

3.1. The Seasonal Cycle

An interesting aspect of the high-latitude site occupied during MLML was that despite the relatively short duration of the moored record (just over 4 months), the data included both the spring and fall transitions in upper ocean stratification. The spring transition is when upper ocean restratification is initiated after deep winter mixing, and the fall transition is when the mixed layer begins deepening again. These changes in stratification are associated with the seasonal transitions in heat flux from negative (heat loss from the ocean) to positive and vice versa. Climatological data for the region [*Isemer and Hasse*, 1987] show that the air-sea temperature difference and surface wind are good indicators of the seasonal transitions. The air minus sea temperature changes from negative to positive in late May and from positive to negative in mid-August. Wind speed decreases

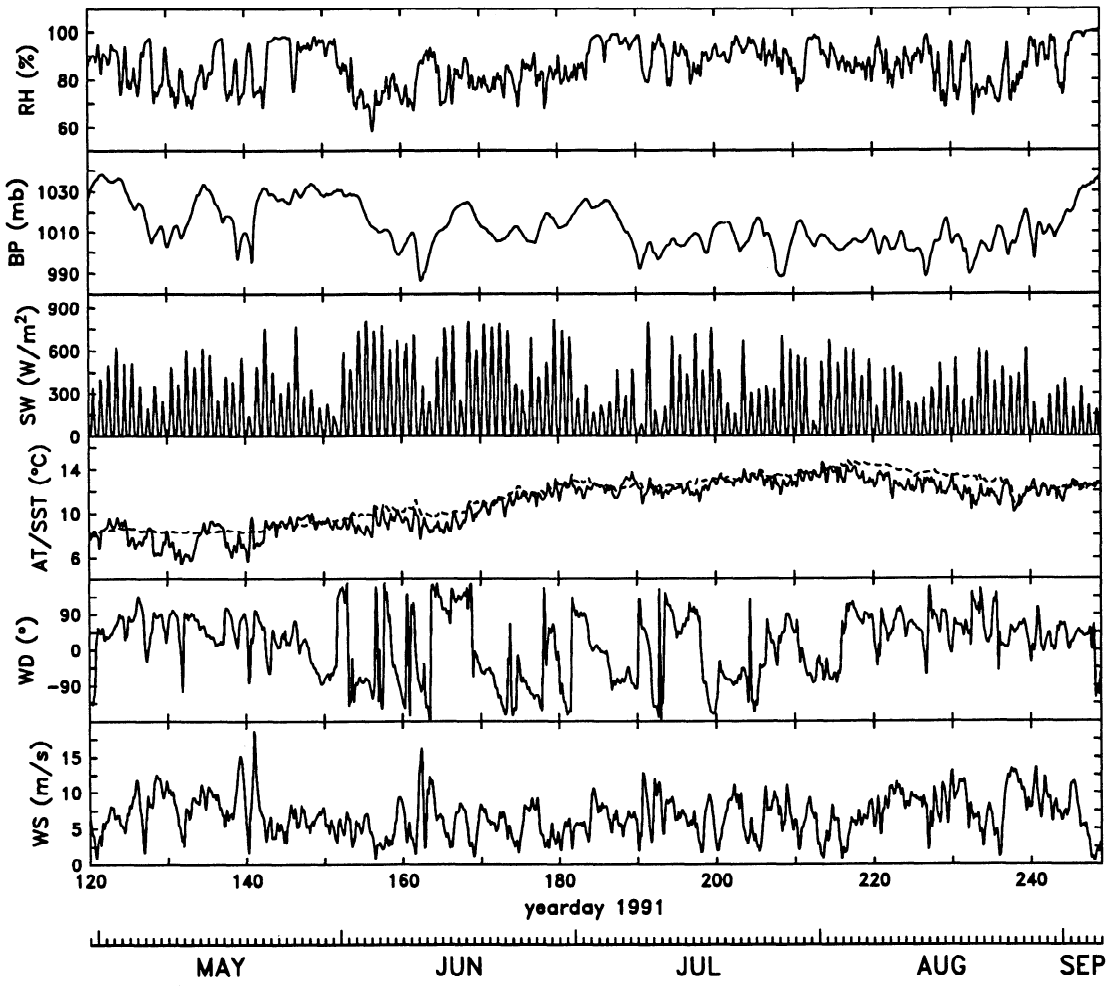

Figure 4. The final meteorological data set, determined to be the best available observations from the two VAWR's [*Plueddemann et al.*, 1993]. The original 15-min data have been smoothed over 4 hours and plotted every 2 hours. The variables are, from top to bottom, relative humidity (RH), barometric pressure (BP), incident shortwave radiation (SW), air temperature (AT, solid curve) and sea surface temperature (SST, dashed curve), wind direction (WD), and wind speed (WS).

rapidly throughout April and May, reaching a plateau near 8 m s^{-1} from June to mid-August. In September, wind speed begins a rapid increase. Monthly mean wind speeds in winter are typically 13–18 m s^{-1} [*Lambert and Hebenstreit*, 1985; *Isemer and Hasse*, 1987]. Wind direction tends to be relatively steady toward the northeast during the winter months and more variable in summer.

Comparison of the meteorological data from the mooring with the climatology sets the context for the seasonal transitions observed during the MLML experiment. Of course, the MLML mooring data are much more variable than the multiyear climatological means, and the actual transitions tend to be episodic. Still, the spring and fall transitions are apparent in the MLML meteorological data (Figure 4). Relatively persistent, negative air-sea temperature differences with magnitudes of 1.5°–2°C are seen up until about May 22 and after August 5. In the intervening period both air and sea temperatures show a warming trend, and their difference is typically less than 1°C. Wind direction is relatively steady toward the northeast until May 26 and after August 3, with more variability in the intervening period. The mean wind speed is about 8 m s^{-1} during May and August, but only about 6 m s^{-1} during June and July. To facilitate discussion of seasonal variation, we have defined the effective dates of the spring and fall transitions to be May 22 and August 5, respectively.

Daily averages of the wind stress, heat flux components, and total heat flux are shown in Figure 5. Seasonal variability is most apparent in the wind stress and in the sensible and latent heat fluxes. The wind stress averaged over the spring and fall periods is about 0.15 N m^{-2}, dropping to 0.08 N m^{-2} in summer. Sensible and latent heat fluxes have means of -13 and -41 W m^{-2}, respectively, over the spring and fall periods, but only -7 and -25 W m^{-2} during summer. In general, the observed seasonal means compare well with climatology for the region [*Isemer and Hasse*, 1987]. The principal exceptions are that the observed seasonal variation in wind stress is more pronounced than the climatological variation (larger May and August stresses in the observations) and the observed net shortwave radiation in June is significantly larger than the June mean from climatology.

The seasonal variation in surface forcing drives the cycle of mixed layer deepening and restratification which dominates the vertical structure of the upper ocean in the subarc-

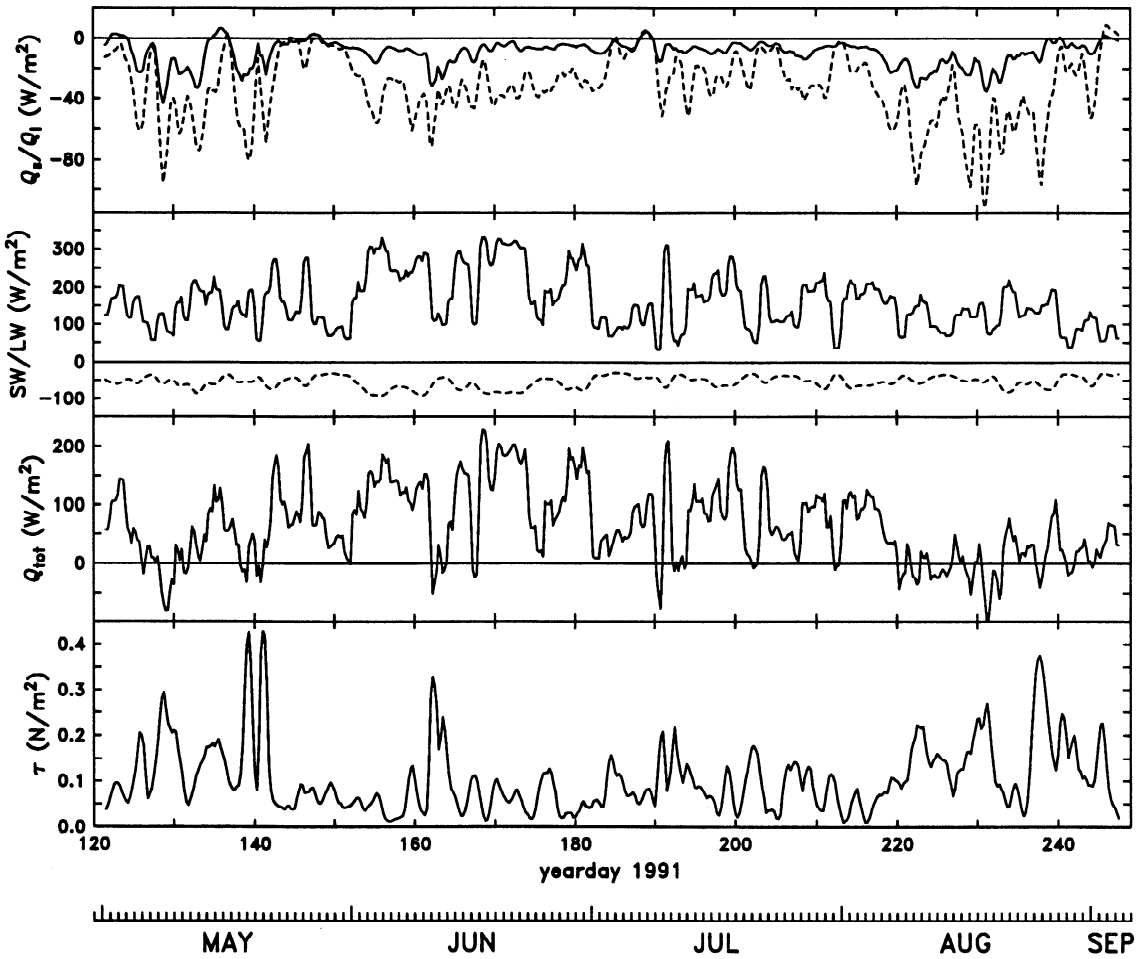

Figure 5. Bulk air-sea fluxes for MLML. The fluxes were computed from the 15-min meteorological variables but have been smoothed over 24 hours prior to plotting. The four panels show (from top to bottom) sensible (solid curve) and latent (dashed curve) heat flux, net shortwave (solid curve) and net longwave (dashed curve) radiation, total heat flux, and wind stress magnitude. The sign of the heat fluxes is positive for a heat gain by the ocean.

tic North Atlantic. This cycle is clearly seen in the temperature profiles from Ocean Weather Station India (OWSI, 59°N, 19°W, Figure 1) analyzed by *Lambert and Hebenstreit* [1985]. Weekly bathythermograph (BT) profiles were available for the upper 125 m of the water column over a 10-year period (1965–1974) at OWSI, within about 100 km of the MLML mooring site. The 10-year mean seasonal cycle in temperature is shown in Figure 6 along with the observations from the MLML mooring. The OWSI winter surface temperature is near 9°C, and the near equality of SST and 125-m temperature indicates a deep (>125 m) mixed layer from January to early April. Summer warming results in an increase of about 1°C at 125 m and almost 4°C at the surface. The 118-m temperature from the MLML mooring is about 1°C cooler than the OWSI 125-m temperature but shows a similar increase from May through August. In contrast, the MLML SST shows a more pronounced warming (ΔT = 6°C) than the OWSI SST. In fact, the MLML restratification, measured by the SST minus 118-m temperature difference, is more dramatic than any individual year in the OWSI record. The anomalously large June net shortwave radiation observed at the MLML mooring may be responsible for the large SST increase.

More complete documentation of the observed temperature variability is shown in Plate 1, where the MLML temperature data have been contoured versus depth and time. Significant surface warming begins at the spring transition (May 22) and continues up to the fall transition (August 5). Strong stratification develops between 20 m and 50 m through July and into August, with the most intense warming confined to the upper 15 m. Although previous analyses in the region [*Gill*, 1975; *Lambert and Hebenstreit*, 1985; *Stramska and Dickey*, 1994] indicated that the dominant temperature signal at the MLML site would be seasonal variability driven by local surface fluxes, the effects of mesoscale variability can also be seen. For example, the strong seasonal stratification isolates the deep water (>80 m) from the surface, and it is unlikely that the variations in the 7.5°–9°C water after about June 17 are due to local surface processes. Similarly, isotherm displacements in the strongly stratified layer during July 15–25 and August 25–27 are unlikely to be explained by local forcing.

Frequency spectra (Figure 7) computed from the moored current records indicate that the velocity field was dominated by low-frequency (days to weeks) variability plus oscillations at inertial and tidal periods. Separate peaks can

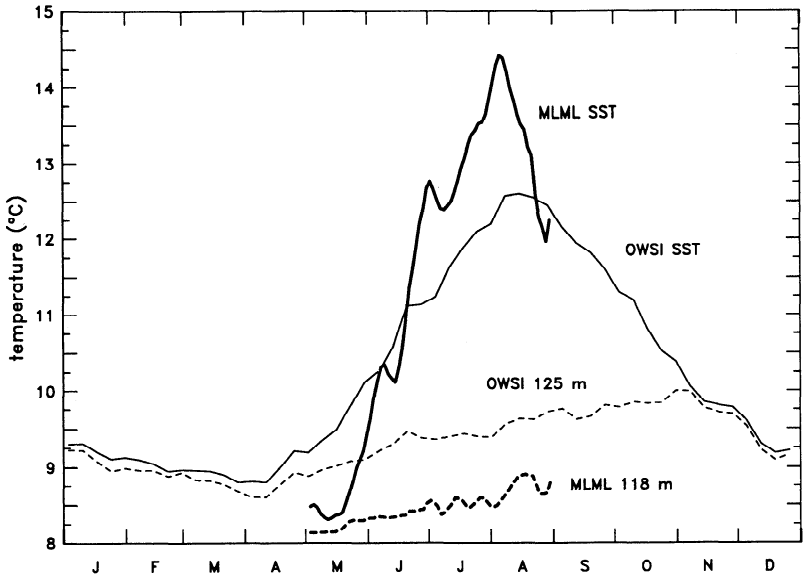

Figure 6. The seasonal cycle of temperature variation at Ocean Weather Station India (OWSI) compared with observations from the MLML mooring. The OWSI data are 10-year means (1965–1974) of weekly average temperatures at the surface and 125 m. MLML temperatures from the surface and 118 m have been averaged to 1 week for comparison.

be detected near the local inertial (0.07 cph) and semidiurnal tidal (0.08 cph) frequencies in the deeper spectra. The low-frequency variability is evident in the vector "stick plots" of daily averaged velocity at selected depths shown in Figure 8. It is clear from the figure that the currents are highly coherent with depth over the upper 300 m. The 10-m record does show some deviation from the pattern in the deeper records, presumably as a result of the local response to surface winds. During the spring and fall periods, velocity magnitudes are from 20 to 40 cm s^{-1} and directions are relatively steady for days to weeks at a time. During summer the currents are substantially weaker (10–20 cm s^{-1}) and more variable. Major current transitions occur on May 7, May 15, and August 26.

An assessment of advective variability at the mooring site would require knowledge of horizontal temperature gradients, but these were estimated only during spring and fall survey cruises (B. H. Jones et al., Spatial variability, turbulent mixing, and phytoplankton productivity in the North Atlantic Ocean south of Iceland in August 1991, submitted to *Journal of Geophysical Research*, 1994; hereinafter referred to as submitted manuscript). As a guide to the interpretation of temperature variability during the seasonal cycle, the observations were compared to a simple one-dimensional model (*Price et al.* [1986]; hereafter PWP). The PWP model parameterizes vertical mixing and restratification as processes driven solely by the local surface fluxes of heat and momentum [e.g., *Niiler and Kraus*, 1977] in order to predict the vertical structure of temperature, salinity, and velocity. The surface fluxes are prescribed from observations and are assumed to enter or leave the ocean in the uppermost model layer except for insolation, which is absorbed within the water column. Three vertical mixing processes are parameterized. Free convective mixing, mixed layer entrainment, and the effects of shear flow instability are simulated using a static stability criterion, a bulk Richardson number, and a gradient Richardson number, respectively. The latter two processes can be considered parameterizations of wind mixing in the sense that the model velocity shear that appears in the Richardson numbers is entirely wind driven. The use of both bulk and gradient Richardson number criteria allows for a smooth transition at the mixed layer base.

For MLML the model was run with a vertical resolution of 1 m and a time step of 15 min. The bulk fluxes derived from the MLML meteorological data defined the surface forcing necessary to drive the model. At each time step, solar radiation was absorbed within the upper ocean, while the sensible, latent, and net longwave heat fluxes were applied at the uppermost level. The freshwater flux (i.e., salinity change) from the estimated precipitation time series was included in the model, but the heat and momentum fluxes due to rain were not. The density profile was calculated at each time step and, if necessary, adjusted to achieve static stability. Wind stress was then absorbed within the mixed layer, and the momentum balance was stepped forward in time. The bulk Richardson number was calculated at each depth, and the mixed layer entrained downward until bulk stability was satisfied. The gradient Richardson number was then calculated over the stratified portion of the profile (below the mixed layer) until stability was achieved throughout the stratified region. There were no significant differences between this implementation and that described by PWP. The decay scale (e-folding time) for inertial oscillations in the model mixed layer was taken to be 4 days, which produced a good match with the observations. The penetration of solar radiation was parameterized using the *Paulson and Simpson* [1977] scheme for type II water. The model was initialized with temperature and salinity profiles from the predeployment CTD cast.

The observed and modeled SST are compared in Figure 9. The relative success of the model prediction prior to the spring transition (May 22), and comparative lack of success after the fall transition (August 5), is striking. The model

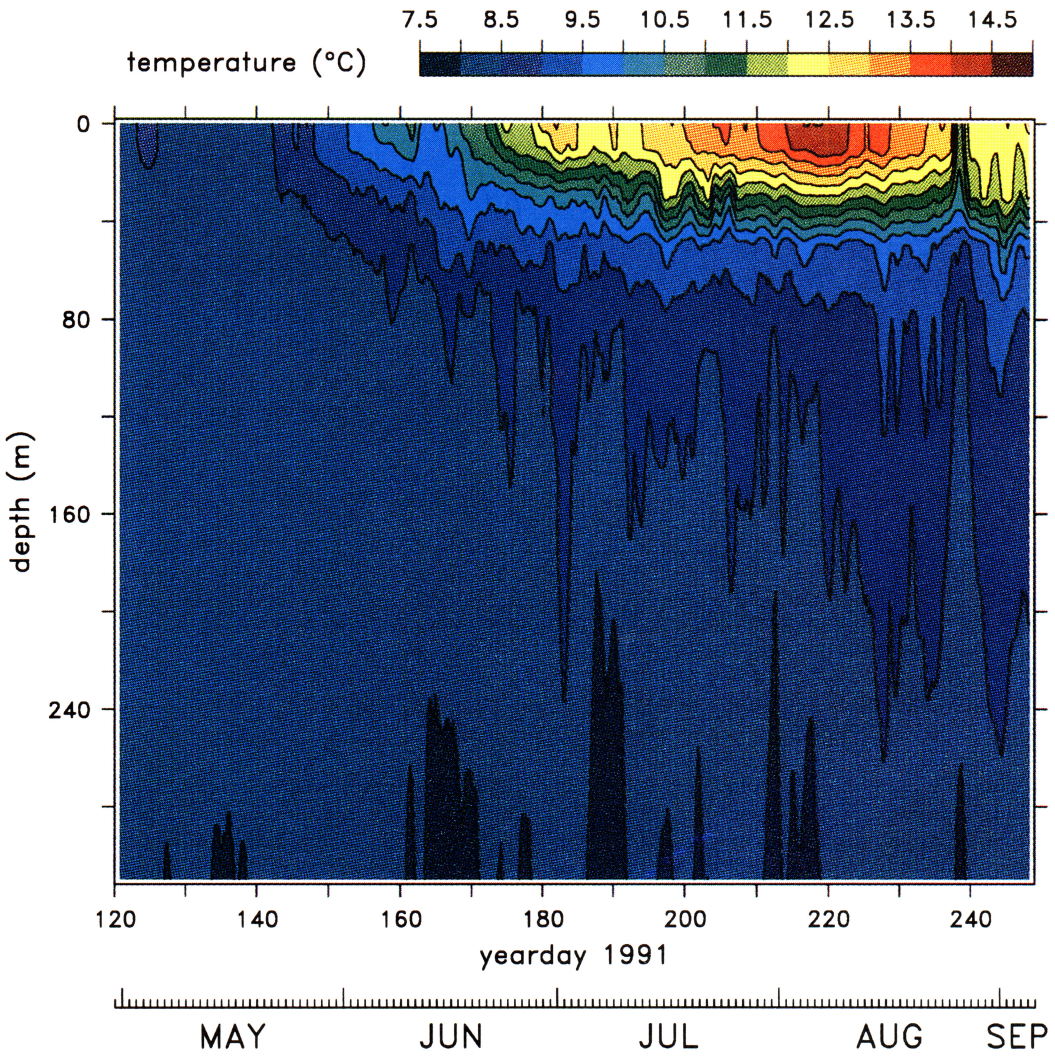

Plate 1. Contour plot of temperature from the MLML mooring. The data, collected at 15-min intervals, have been smoothed over 1 day. The spring transition (May 22) and subsequent upper ocean restratification can be clearly seen. The fall transition (August 5) marks the beginning of surface cooling and the breakdown of stratification.

predicts SST within a few tenths of a degree during most of May despite the presence of strong, variable currents (Figure 8). It is likely that this is because horizontal temperature gradients were small, perhaps as a result of upper ocean homogenization by winter storms. After the fall transition, the slope (time rate of change) of the modeled SST is persistently different than that of the observations, and large, transient features are observed that are not present in the model. This behavior can be contrasted to that during the summer warming period, where the observed slope and variability are generally well modeled and the comparison would likely be improved if the model could be reinitialized after a few abrupt events (e.g., July 12).

The ability of the one-dimensional model to make a reasonable prediction of SST over several months (within about 0.5°C up to August 1) while the absolute temperature increased substantially (≈6°C) indicates that local forcing and vertical processes dominated the spring transition and summer warming periods. Assessing the poor performance of the model after the fall transition is more problematic, since discrepancies between model and observations may be due to any process not included, or improperly parameterized, in the model. However, it is likely that the recurrence of strong currents (Figure 8) in the presence of large temperature gradients (B. H. Jones et al., submitted manuscript, 1994) increased the importance of advection. In fact, the largest unmodelled temperature variations during this period appear to be linked to current fluctuations at low frequency (the ocean mesoscale), as can be seen from the correspondence between the reversal in current from northward to southwestward from August 25 to 27 (Figure 8) and a dramatic temperature decrease at all depths (Plate 1).

3.2. The Initiation of Restratification

Although the general agreement of the observed fluxes with seasonal climatology is reassuring, it is important to recognize that isolated, local events tend to dominate the record. For example, four major storms associated with low barometric pressure and strong winds ($\tau > 0.15$ N m^{-2}) can be identified in the meteorological record (Figure 6 and Plate 1), two occurring before the spring transition (May 7–10 and 18–21) and two afterward (June 11–12 and July 9–11). The

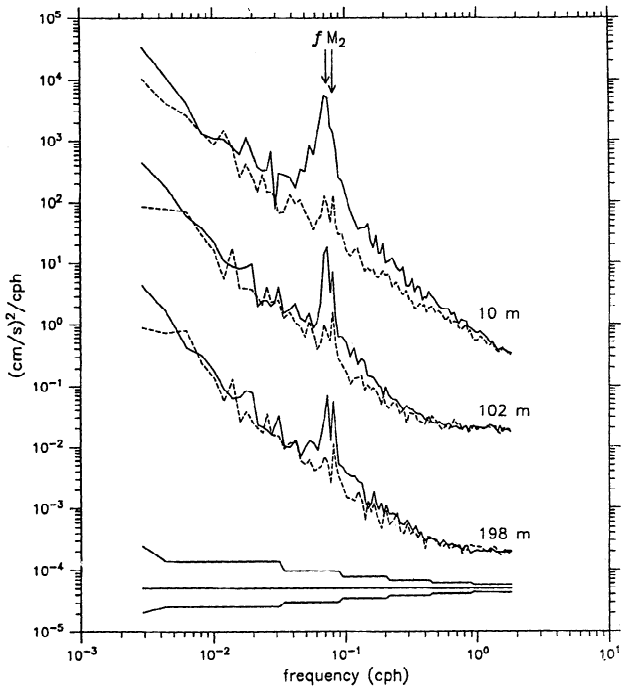

Figure 7. Rotary spectra of clockwise (solid curve) and anticlockwise (dashed curve) velocity components from the MVMS at 10-m depth and ADCP depth cells at 102 and 198 m. Low-frequency ($f < 0.03$ cph) energy and a near-inertial peak ($f = 0.07$ cph) dominate the spectra. Note that the MVMS spectra show a consistent high-frequency slope, while the ADCP spectra begin to level out at about 0.3 cph due to instrumental noise. Deeper spectra have been offset by 10^{-2} for clarity.

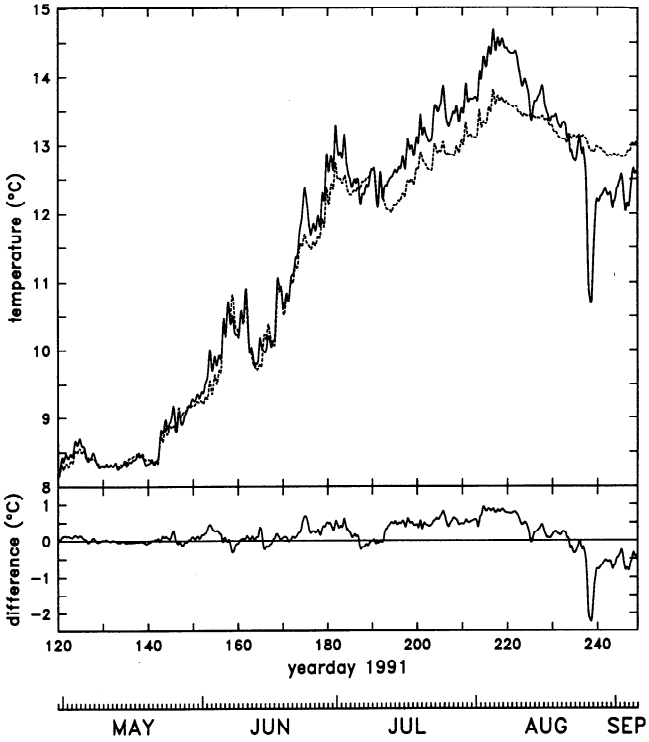

Figure 9. Comparison of observed and modeled SST. The upper panel shows the observed SST at the MLML mooring (solid curve) and the prediction of the PWP mixed layer model (dashed curve). The lower panel shows the SST difference (observed − model). Data have been smoothed over 12 hours.

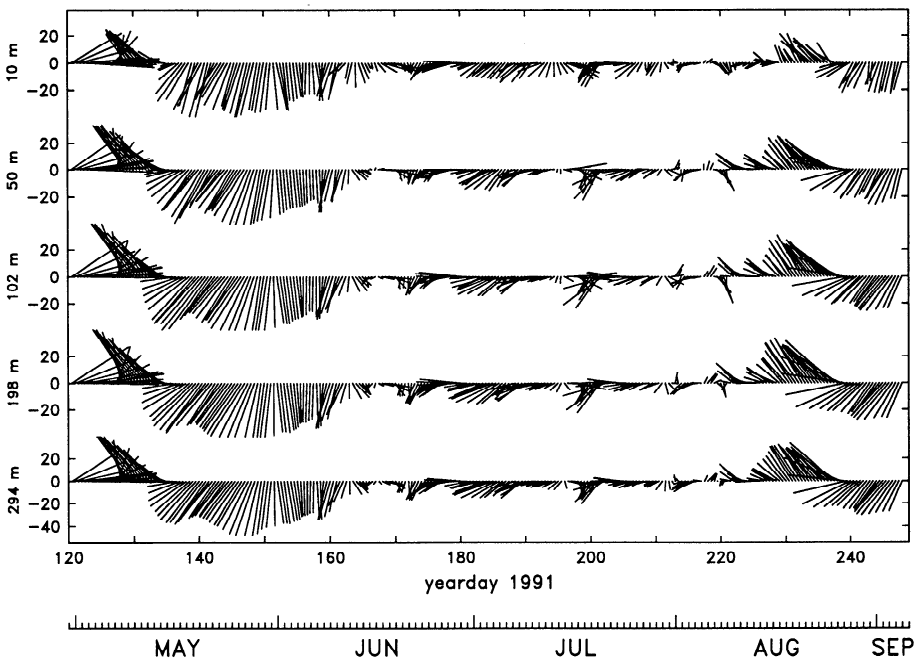

Figure 8. Vector "stick plots" of velocity from selected depths on the MLML mooring. The five panels, from top to bottom, show currents in cm s^{-1} from depths of 10, 50, 102, 198, and 294 m. The data have been averaged over 1 day and are plotted every 12 hours. A stick pointing to the top of the figure represents a northward flowing velocity.

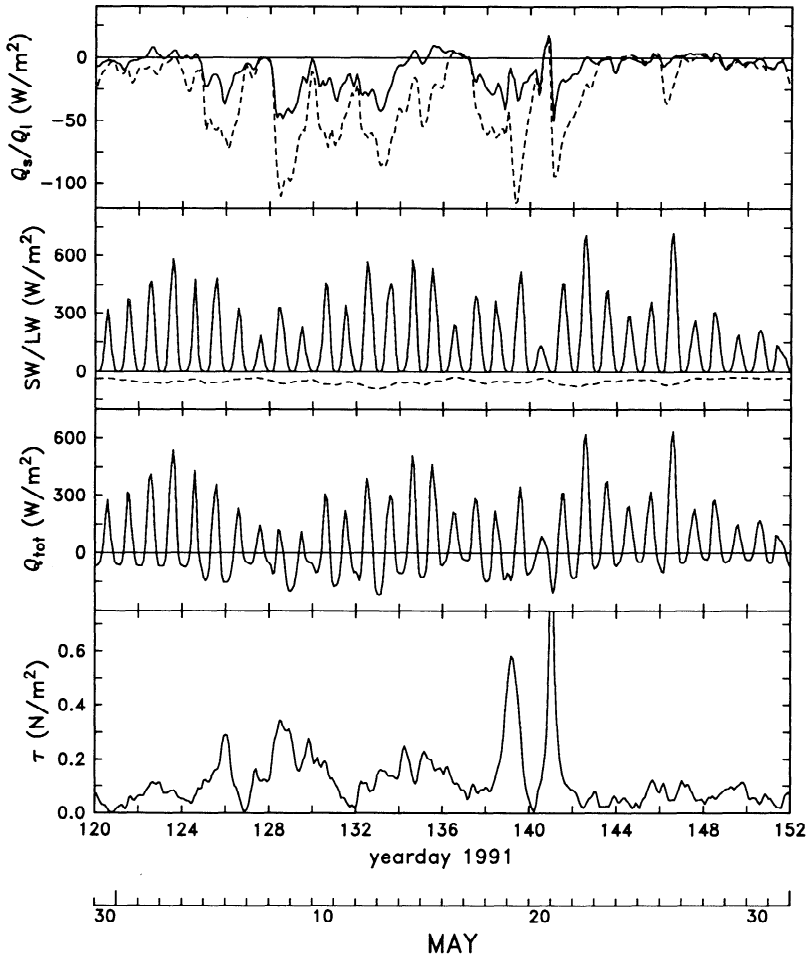

Figure 10. Time series of air-sea fluxes during May. The period from May 5 to 21 is characterized by substantial sensible and latent heat losses due to strong winds and cold, dry air at the sea surface. The total heat flux has pronounced positive to negative oscillations and a mean of only 20 W m^{-2} into the ocean during this period. The 15-min data have been smoothed over 4 hours. The 15-min average wind stress on May 21 reached a peak of 1.7 N m^{-2}.

May 18–21 storm was the strongest, with peak winds of just over 22 m s^{-1} observed at the mooring and a strong signature in the sensible and latent heat fluxes. Of particular interest for this study is the fact that variability in the local surface forcing results in an episodic transition to the spring warming phase.

Figure 10 shows time series of the meteorological variables for the period April 30 to May 31 when restratification was initiated. Plate 2 shows contours of temperature versus depth and time for the same period as the fluxes in Figure 10. The water column was initially very well mixed, with a temperature difference of less than 0.07°C between the surface and 250-m depth. However, restratification began almost immediately during a period of uncharacteristically weak winds from April 30 to May 4. A "thermal cap" was formed in the upper 50 m with a vertical temperature gradient of about 0.5°C. This surface stratification was homogenized down to about 40 m by the May 5–6 wind event. The period from May 5 to 21 was one of pronounced positive to negative oscillations in total heat flux, with peak values averaging −130 W m^{-2} at night versus 270 W m^{-2} during the day, and a mean flux of only 20 W m^{-2} into the ocean. This period was characterized by episodic restratification and mixing, manifested as alternate warming and cooling of the upper 60 m of the water column (Plate 2). The period of strong diurnal near-surface temperature variability ended after the strong storm on May 18–21, and the surface stratification initiated on May 22 continued to intensify until the fall transition on August 5 (Plate 1).

Temperatures from the PWP model are shown in Plate 3 for comparison with the observations (this is the subsurface temperature field from the same model run used for the SST comparison shown in Figure 9). The one-dimensional model is successful, in that the timing and extent of principal features in the upper 100-m temperature field are reproduced. The thermal cap from April 30 to May 4, the period of weak, variable stratification from May 5–21, and the onset of restratification on May 22 can be seen in Plate 3. The observed isotherm depths show high-frequency variability which does not appear in the model isotherms. This is presumably due to the vertical motions of internal waves and tides which are not included in the model. Still, prior to May 22 the observed and modeled temperatures agree to within about 0.1°C above 100 m. Larger discrepancies after May 22 result from low-frequency oscillations in the observed isotherm depths (e.g., the 70-m excursion of the 8.3°C isotherm

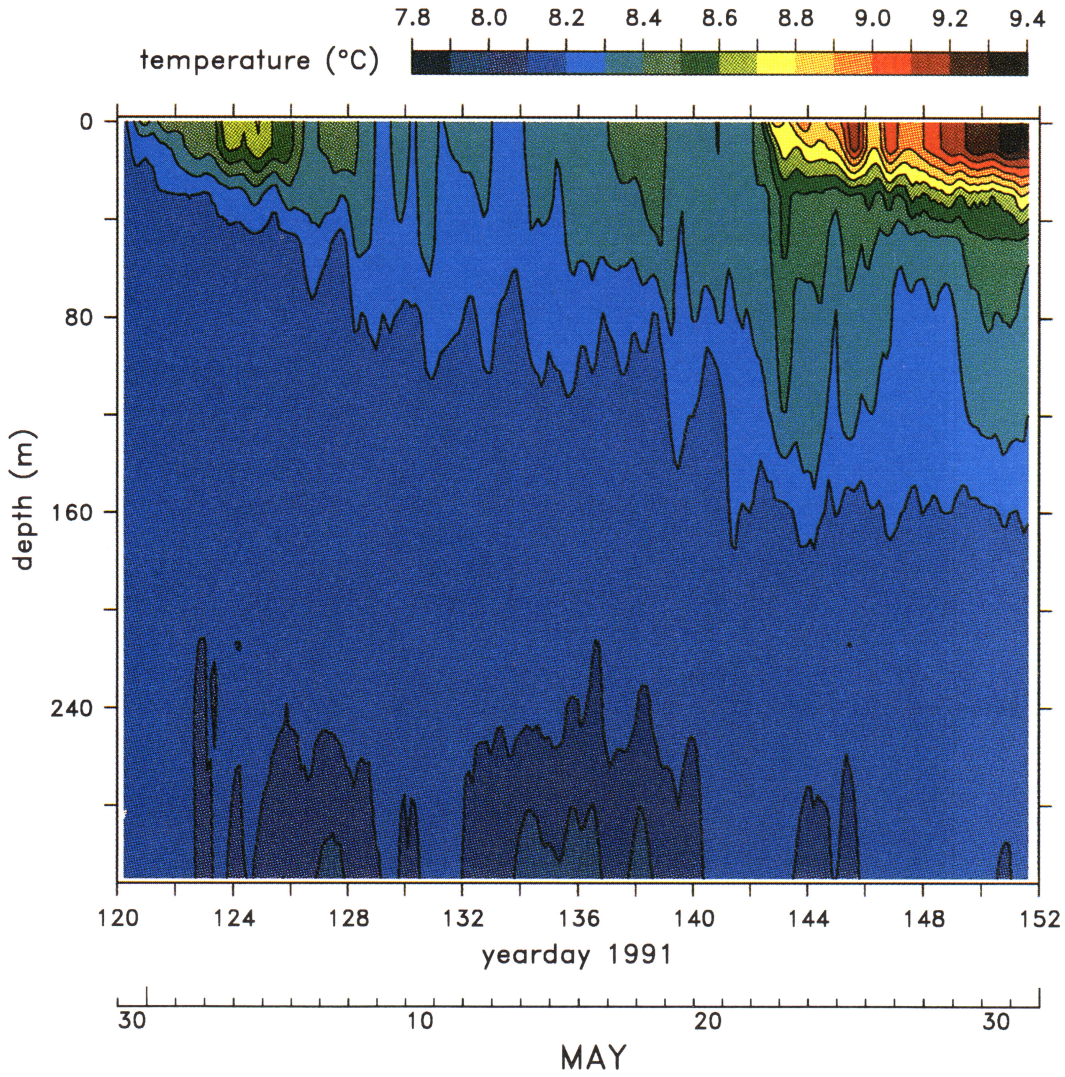

Plate 2. Contour plot of observed temperature for the period April 30 to May 31. A developing "thermal cap" can be seen between May 1 and 5, giving way to episodic mixing and restratification from May 5 to 21. The "permanent" seasonal stratification is initiated on May 22. The 15-min data have been smoothed over 12 hours.

from May 23–27). The most significant difference between the observed and modeled temperature is that the apparent depth of heat penetration in the observations is greater than that in the model. This can be seen by comparing the depths of the 8.2°C isotherms. This difference may be due to insufficient vertical mixing in the model, the influence of horizontal advection, or other processes not included in the model (e.g., the phytoplankton bloom [*Stramska and Dickey*, 1993]).

The role of horizontal advection during restratification can be addressed in part by consideration of the shipboard survey carried out from May 6 to 9. The survey mapped temperature, salinity, and bio-optical variables within an approximate 100 km by 100 km square centered on the MLML mooring. The temperature field at 50-m depth (Figure 11) shows gradients oriented predominantly from northeast to southwest. The strongest gradients ($\Delta T \approx 0.5$°C over 25 km) were southwest of the mooring. The northwest to southeast gradients were substantially weaker (<0.2°C across the survey region). The temperature field at depths as shallow as 20 m and as deep as 150 m showed similar northeast to southwest oriented gradients, with isotherms widely spaced to the northeast and more closely packed to the southwest of the mooring. The magnitude of the gradients was largest near 50-m depth. The interpretation below is based on the assumptions that the survey provides synoptic maps of the 10- to 100-km temperature field, and that it is appropriate to consider these maps to be advected as a frozen field. The assumption of synopticity appears reasonable, since the location, orientation, and magnitude of the strongest gradients was persistent over the 4-day period. The frozen field assumption is reasonable to the extent that the apparent advective temperature changes occur while the flow is steady in magnitude and direction (i.e., temperatures and currents are not in a thermal wind balance).

At the start of the survey, currents were toward the east (Figure 8). Cross-gradient currents during May 6–8 could have resulted in temperature increases of 0.2°–0.3°C at the mooring. There is a hint of this effect in the observations, as pulses of warm water appear between 30 and 90 m and the

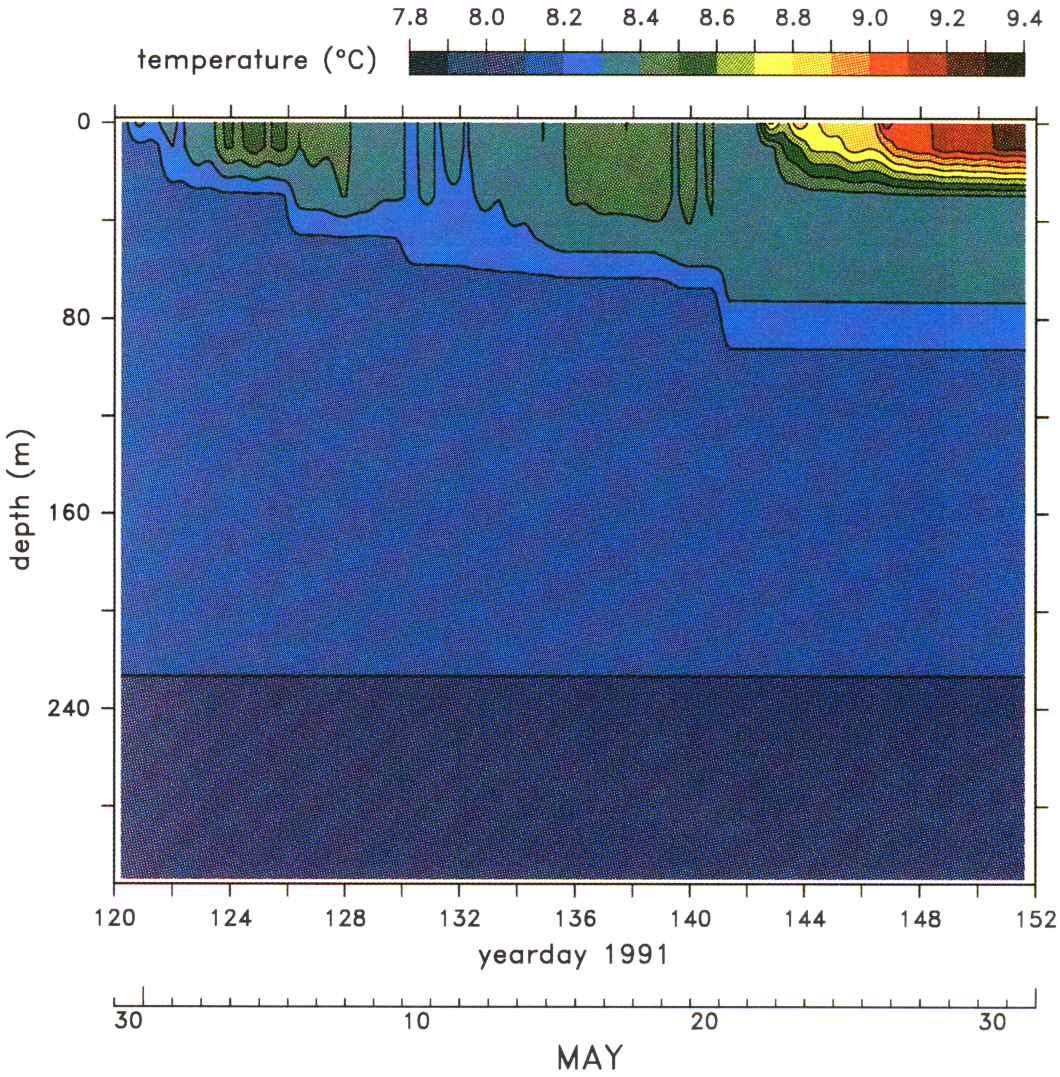

Plate 3. Contour plot of temperature from the output of the PWP mixed layer model for the period April 30 to May 31. The principal features of the observed temperature in the upper 100 m (Plate 2) are reproduced.

8.2°C isotherm deepens more rapidly than that of the model. From May 9–14, currents were predominantly along-gradient, and advective variability of a tenth of a degree or less would be expected at the mooring. This is consistent with the fact that the difference between observed and modeled temperature was relatively constant over this period. By May 16, currents had shifted to the southwest. The spatial gradients observed during the survey indicate that cooler water may have been advected past the mooring. This is consistent with the observed shoaling of the 8.3°C isotherm and surface warming which was less pronounced than that of the model from May 14 to 18. After May 22 the discrepancies between observed and modeled temperatures increased, but use of the May 6–9 temperature field to assess advection becomes increasingly questionable.

The 12-hour smoothing, along with the contour intervals chosen for Plates 2 and 3, tend to suppress the details of the vertical temperature structure associated with the period of strong diurnal oscillation in the surface heat flux. However, the observed mixed layer depth clearly showed a change in character during this period (Figure 12; see also *Stramska et al.* [this issue]). Before May 7 and after May 21 the observed mixed layer was shallow (<30 m) and relatively stable. During the period of oscillatory surface heat flux the mixed layer showed a strong diurnal cycle, with depths varying from <20 to 50 m. The model mixed layer variability (Figure 12) is of interest because the mixed layer depth variation can be shown at the 1-m vertical resolution of the model and the strong diurnal oscillations from May 10–21 are more clearly seen. The similarity of the model response to that of the observed mixed layer supports the supposition that the mixed layer depth variability was principally a consequence of local forcing.

The importance of variability in the vertical structure of temperature to bio-optical variability is evident in the analysis of *Stramska et al.* [this issue]. In comparison with similar data from the same site during the spring of 1989 [*Dickey et al.*, 1994a], the phytoplankton bloom occurred a few weeks earlier and resulted in higher chlorophyll concentrations. Defined in terms of vertically integrated Chl_a, the 1991 bloom started during the development of the thermal cap on May 3 and persisted until May 19. The increase in

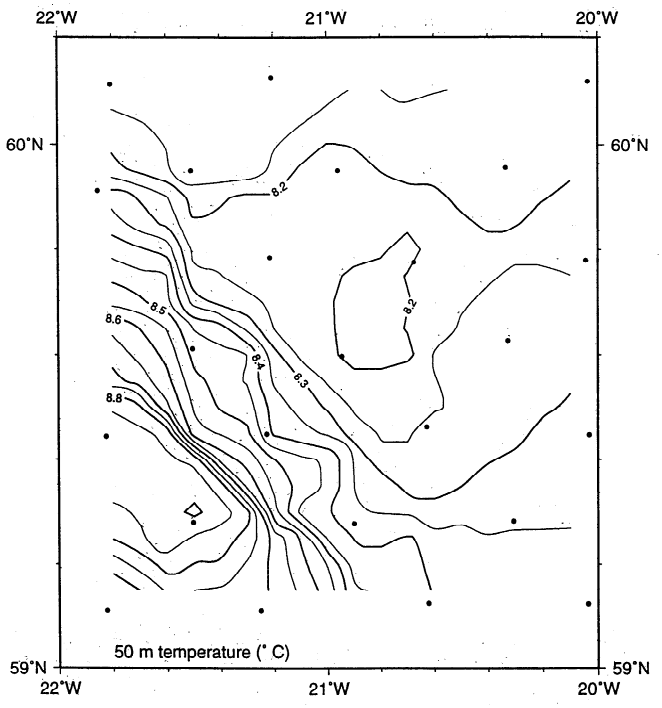

Figure 11. The temperature field at 20-m depth mapped from the shipboard survey carried out during May 6–9, 1991. Solid circles indicate positions of the CTD casts. The mooring was near the center of the survey region (59°35.61′N, 20°57.85′W). The survey started from the position nearest the mooring location, proceeded in an anticlockwise spiral, and ended in the northwest corner.

Chl_a was seen as deep as 90 m during this period. A secondary bloom was observed coincident with the onset of restratification on May 22, but with much less vertical extent and a reduced contribution to the vertically integrated Chl_a in comparison to the initial bloom. The result was that the principal increase in phytoplankton biomass, i.e., the most intense bloom, occurred not after development of the seasonal stratification, but during the period when the mixed layer was relatively deep and showed substantial diurnal variability.

4. Summary and Conclusions

The measurements from the MLML mooring documented the surface forcing and upper ocean response at a high-latitude, severe environment site over a 129-day period (April 30 to September 6) which included the principal seasonal transitions in thermal stratification. The water column was initially well mixed, but restratification began soon after the start of the observations. May 22 (defined as the spring transition) marked the establishment of strong stratification in the upper 100 m, which continued to intensify until August 5 (the fall transition). As measured by the SST minus 118-m temperature difference, the observed seasonal restratification (ΔT = 6°C) was more intense than any in the 10-year record from OWSI [*Lambert and Hebenstreit*, 1985]. Previous observations near the MLML site [*Gill*, 1975; *Lambert and Hebenstreit*, 1985; *Stramska and Dickey*, 1994] indicated that the dominant temperature signal would be seasonal variability driven by local surface fluxes.

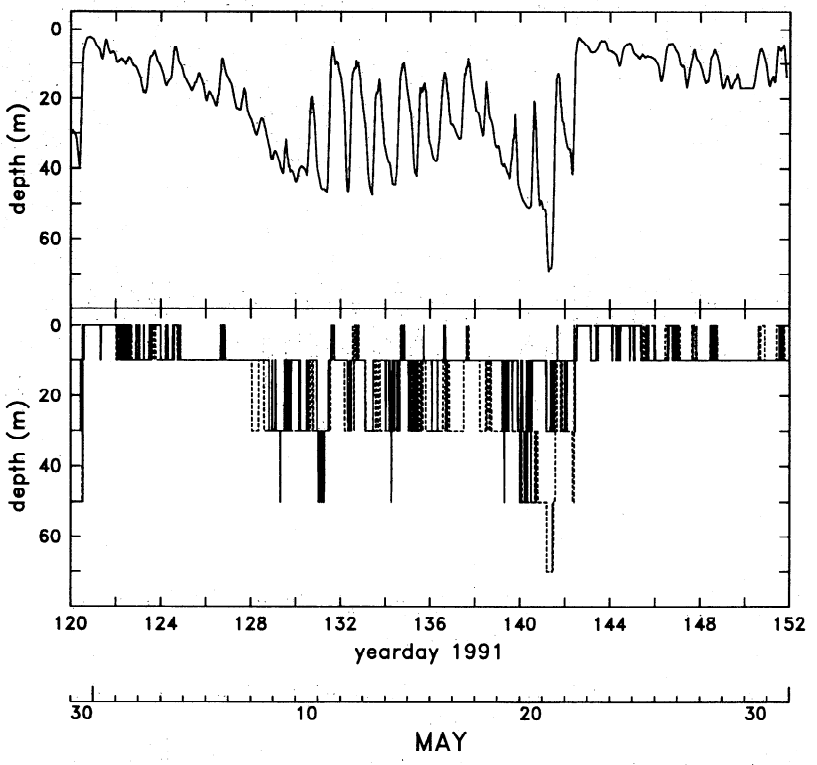

Figure 12. Mixed layer depth, defined as the depth where temperature is 0.01 cooler than the surface temperature, from observations and from the PWP model. The model had a vertical resolution of 1 m, resulting in a smooth mixed layer depth time series (upper panel). Observations were available only at 10, 30, 50, 70, and 80 m, resulting in a "stepped" time series (lower panel, solid line). The model shows similar behavior when subsampled at the same depths as the observations (lower panel, dashed line).

This was confirmed by the comparison of observed SST to that predicted by the one-dimensional mixed layer model (PWP). The ability of the model to reproduce the general trend and many of the detailed features of SST variability, along with the small differences in magnitude between observed and modeled SST ($\Delta T < 0.5$°C), indicated that local processes dominated during the initiation of restratification and during the summer warming period. After the fall transition, however, neither the magnitude nor the slope of the SST variations was well predicted by the model. It was presumed that this was principally the result of nonlocal processes such as horizontal and vertical advection.

Of particular interest was the initiation of restratification in May. The water column was initially well mixed, but restratification began almost immediately, forming a "thermal cap" in the upper 50 m during May 1–5. The period from May 5 to 21 was one of pronounced positive to negative oscillations in total heat flux, with a mean flux into the ocean of only 20 W m^{-2}. This resulted in breakdown of the thermal cap, followed by alternating development and destruction of stratification and intense diurnal cycling of the mixed layer depth. Increasing heat fluxes and weakening winds after May 22 caused the initiation of "permanent" seasonal stratification, which continued to intensify until the fall transition. A shipboard CTD survey provided a snapshot of the horizontal temperature gradients during May 6–9, and a qualitative assessment indicated that advective variability at the mooring would be small. Indeed, both SST and the subsurface temperature structure from the one-dimensional model agreed with the observed temperatures to within about 0.1°C prior to May 22. After May 22 the discrepancies between observed and modeled temperatures increased, and the lack of concurrent information about horizontal temperature gradients precluded an assessment of advective processes. Still, the one-dimensional model reproduced the thermal cap, the period of mixed layer depth variability, and the onset of seasonal stratification. It was concluded that the observed vertical variability in temperature was strongly controlled by local surface forcing during this period.

Acknowledgments. The MLML mooring was designed, deployed, and recovered by the Upper Ocean Processes Group (UOPG) at the Woods Hole Oceanographic Institution. Field operations were facilitated by the captain and crew of the R/V *Endeavor*. The VAWR, ADCP, and STL's were prepared, calibrated, and analyzed by the UOPG. Three MVMS's (30, 70, and 90 m) were prepared and processed by the Lamont Doherty Earth Observatory, and two (10 and 50 m) by the Ocean Physics Group at the University of Southern California. MVMS current and temperature data were analyzed by the UOPG. Temperature data from the shipboard survey was provided by L. Washburn and B. Jones. This work was funded by codes 1122SS and 1123B of the Office of Naval Research under grants N00014-89-J-1683 (A.J.P., R.A.W.), N00014-J-89-1498 (T.D.D., M.S.), and N00014-89-J-1150 (J.M.). Woods Hole Oceanographic Institution contribution 8662.

References

Clarke, N. E., L. Eber, R. M. Laurs, J. A. Renner, and J. F. T. Saur, Heat exchange between ocean and atmosphere in the eastern North Pacific for 1961–71, *NOAA Tech. Rep., NMFS SSRF-682*, 1974.

Dean, J. P., and R. C. Beardsley, A vector-averaging wind recorder (VAWR) system for surface meteorological measurements in CODE (Coastal Ocean Dynamics Experiment), *Tech. Rep. WHOI-88-20*, 74 pp., Woods Hole Oceanogr. Inst., Woods Hole, Mass., 1988.

Dickey, T. D., The emergence of concurrent, high-resolution physical and bio-optical measurements in the upper ocean and their applications, *Rev. Geophys.*, *29*, 383–413, 1991.

Dickey, T. D., J. Marra, T. Granata, C. Langdon, M. Hamilton, J. Wiggert, D. Siegel, and A. Bratkovich, Concurrent high-resolution bio-optical and physical time series observations in the Sargasso Sea during the spring of 1987, *J. Geophys. Res.*, *96*(C5), 8643–8663, 1991.

Dickey, T. D., et al., Seasonal variability of bio-optical and physical time series observations in the Sargasso Sea, *J. Geophys. Res.*, *98*(C1), 865–898, 1993.

Dickey, T., J. Marra, M. Stramska, C. Langdon, T. Granata, A. Plueddemann, R. Weller, and J. Yoder, Bio-optical and physical variability in the subarctic North Atlantic Ocean during the spring of 1989, *J. Geophys. Res.*, *99*, 22,541–22,556, 1994a.

Dickey, T. D., D. V. Manov, R. A. Weller, and D. A. Siegel, Determination of net longwave heat flux at the air-sea interface using measurements from ship and buoy platforms, *J. Atmos. Oceanic Technol.*, *11*(4), 1057–1078, 1994b.

Ducklow, H. W., Joint global ocean flux study: The 1989 North Atlantic bloom experiment, *Oceanography*, *2*(1), 4–7, 1989.

Fung, I. Y., D. E. Harrison, and A. A. Lacis, On the variability of the net longwave radiation at the ocean surface, *Rev. Geophys.*, *22*, 177–193, 1984.

Gill, A. E., Evidence for mid-ocean eddies in weather ship records, *Deep Sea Res.*, *22*, 647–652, 1975.

Isemer, H. J., and L. Hasse, *The Bunker Climate Atlas of the North Atlantic Ocean*, vol. 1, *Observations*, 218 pp., Springer-Verlag, New York, 1985.

Isemer, H. J., and L. Hasse, *The Bunker Climate Atlas of the North Atlantic Ocean*, vol. 2, *Air-Sea Interactions*, 252 pp., Springer-Verlag, New York, 1987.

Lambert, R. B., and G. T. Hebenstreit, Upper ocean stratification and variability in the North Atlantic, *Tech. Rep. SIAC-84/1778*, 67 pp., Sci. Appl. Int. Corp., McLean, Va., 1985.

Large, W. G., and S. Pond, Open ocean momentum flux measurements in moderate to strong winds, *J. Phys. Oceanogr.*, *11*, 324–336, 1981.

Large, W. G., and S. Pond, Sensible and latent heat flux measurements over the ocean, *J. Phys. Oceanogr.*, *12*, 464–482, 1982.

Marra, J., Marine bioluminescence and upper ocean physics: Seasonal changes in the northeast Atlantic, *Oceanography*, *2*(1), 36–38, 1989.

McGillicuddy, D. J., J. J. McCarthy, and A. R. Robinson, Coupled physical and biological modeling of the spring bloom in the North Atlantic, I, Model formulation and one-dimensional bloom processes, *Deep Sea Res.*, in press, 1995a.

McGillicuddy, D. J., A. R. Robinson, and J. J. McCarthy, Coupled physical and biological modeling of the spring bloom in the North Atlantic, II, Three-dimensional bloom and post-bloom processes, *Deep Sea Res.*, in press, 1995b.

Neilson, D. J., M. I. Latz, and J. F. Case, Temporal variability in the vertical structure of bioluminescence in the North Atlantic Ocean, *J. Geophys. Res.*, this issue.

Niiler, P. P., and E. B. Kraus, One-dimensional models, in *Modeling and Prediction of the Upper Layers of the Ocean*, edited by E. B. Kraus, pp. 143–172, Pergamon, New York, 1977.

Paulson, C. A., and J. J. Simpson, Irradiance measurements in the upper ocean, *J. Phys. Oceanogr.*, *7*, 952–956, 1977.

Payne, R. E., Albedo of the sea surface, *J. Atmos. Sci.*, *29*, 959–970, 1972.

Plueddemann, A. J., R. A. Weller, T. D. Dickey, J. Marra, G. H. Tupper, B. S. Way, W. M. Ostrom, P. R. Bouchard, A. L. Oien, and N. R. Galbraith, The Marine Light–Mixed Layer Experiment cruise and data report, *Tech. Rep. WHOI-93-33*, 116 pp., Woods Hole Oceanogr. Inst., Woods Hole, Mass., 1993.

Price, J. F., R. A. Weller, and R. Pinkel, Diurnal cycling: Observations and models of the upper ocean response to diurnal heating, cooling, and wind mixing, *J. Geophys. Res.*, *91*(C7), 8411–8427, 1986.

Robinson, A. R., et al., Mesoscale and upper ocean variabilities during the 1989 JGOFS bloom study, *Deep Sea Res.*, *40*, 9–35, 1993.

Robinson, M. K., R. A. Bauer, and E. H. Schroeder, Atlas of North

Atlantic–Indian Ocean monthly mean temperatures and mean salinities of the surface layer, *Ref. Publi. 18*, 234 pp., U.S. Nav. Oceanogr. Office, Dep. of the Navy, Washington, D. C., 1979.

Schmitt, R. W., P. S. Bogden, and C. E. Dorman, Evaporation minus precipitation and density fluxes for the North Atlantic, *J. Phys. Oceanogr.*, *19*(9), 1208–1221, 1989.

Smith, R. C., K. J. Waters, and K. S. Baker, Optical variability and pigment biomass in the Sargasso Sea as determined using deep-sea optical mooring data, *J. Geophys. Res.*, *96*(C5), 8665–8686, 1991.

Stramska, M., and T. Dickey, Variability of bio-optical properties of the upper ocean associated with diel cycles in phytoplankton population, *J. Geophys. Res.*, *97*(C11), 17,873–17,887, 1992.

Stramska, M., and T. Dickey, Phytoplankton bloom and the vertical thermal structure of the upper ocean, *J. Mar. Res.*, *51*(4), 819–842, 1993.

Stramska, M., and T. Dickey, Modeling phytoplankton dynamics in the northeast Atlantic during the initiation of the spring bloom, *J. Geophys. Res.*, *99*(C5), 10,241–10,253, 1994.

Stramska, M., T. D. Dickey, J. Marra, A. Plueddemann, C. Langdon, and R. Weller, Bio-optical variability associated with phytoplankton dynamics in the North Atlantic Ocean during spring and summer of 1991, *J. Geophys. Res.*, this issue.

Sverdrup, H. U., On conditions of vernal blooming of phytoplankton, *J. Cons. Int. Explor. Mer*, *18*, 287–295, 1953.

Theriault, K. H., Incoherent multi-beam Doppler current meter performance, Part 1, Estimate variance, *IEEE J. Oceanic Eng.*, *OE-11*(11), 7–15, 1986.

Weller, R. A., D. L. Rudnick, R. E. Payne, J. P. Dean, N. J. Pennington, and R. P. Trask, Measuring near-surface meteorology over the ocean from an array of surface moorings in the subtropical convergence zone, *J. Atmos. Oceanic Technol.*, *7*(1), 85–103, 1990.

T. D. Dickey and M. Stramska, Ocean Physics Group, Department of Earth Sciences, University of Southern California, Los Angeles, CA 90089.

J. Marra, Lamont-Doherty Earth Observatory of Columbia University, Palisades, NY 10964.

A. J. Plueddemann and R. A. Weller, Woods Hole Oceanographic Institution, Woods Hole, MA 02543.

(Received January 7, 1994; revised August 18, 1994;
accepted November 29, 1994.)